April 1987 LRP 320/87

Invited and Contributed Papers
presented at the

1987 International Conference on Plasma Physics
Kiev, USSR - April 6-12, 1987

by the

CRPP Basic Physics Group

INVITED PAPER

INTRINSIC STOCHASTICITY OF PLASMA IONS IN ELECTROSTATIC WAVES

F. Skiff, F. Anderegg, M.Q. Tran, P.J. Paris, T.N. Good,
N. Rynn and R.A. Stern

presented by

F. Skiff

INTRINSIC STOCHASTICITY OF PLASMA IONS IN ELECTROSTATIC WAVES

F. Skiff, F. Anderegg, M.Q. Tran, P.J. Paris, T.N. Good,
N. Rynn* and R.A. Stern+

Centre de Recherches en Physique des Plasmas
Association Euratom - Confédération Suisse
Ecole Polytechnique Fédérale de Lausanne
21, Av. des Bains, CH-1007 Lausanne/Switzerland

Permanent address:

* Department of Physics, University of California at Irvine
Irvine, CA 92717, USA

\+ Department of Astrophysical, Planetary and Atmospheric Sciences, University of Colorado, Boulder, CO 80309, USA

ABSTRACT

We present evidence of intrinsic stochasticity of plasma ions in the field of obliguely propagating electrostatic waves. Experiments are performed in an argon gas dischage as well as in a barium Q machine, and involve the excitation of electrostatic ion cyclotron waves and neutralized ion Bernstein waves using capacitor plate antennas. Changes in the ion distribution function, resolved in space and time, are observed as a function of wave amplitude using laser induced florescence of the ionic states. Plasma wave amplitudes are measured through observation of plasma dielectric motion which is coherent with the applied waves. Concerning the threshold for ion stochasticity, there is close agreement with the predictions of Hamiltonian single-particle theory. Above threshold, however, the waves are influenced by changes produced in the ion distribution function.

1. INTRODUCTION

Wave-particle interactions have long been an issue of fundamental importance in plasma physics. Since exact solutions of such problems are usually very difficult to obtain, one is generally interested in testing the validity of non-self-consistent theory (one which ignores the back reaction of waves on the particle distributions or vice-versa). The incorporation of intrinsic stochasticity into theories of wave-particle interaction presents precisely this kind of problem. By intrinsic stochasticity we mean the apparently chaotic trajectories of particles subject to purely deterministic equations. Because of the complex structure of these chaotic orbits, and their sensitive dependence on initial conditions, a closed form solution of the effect of intrinsically stochastic particle motion on (mean-field) waves has not been found.

That magnetized ions may become stochastic with the application of a single propagating electrostatic wave has been shown theoretically in two contexts. In each case, stochastic motion results when particles are in a region of phase space where the trapping regions of at least two resonances are wide enough (considered separately) that they overlap.[1-2] Smith and Kaufman[3] consider the case of an obliquely propagating wave where the resonances of interest are the cyclotron resonances. Fukuyama,[4] and Karney and Bers[5] consider particle motion in a wave propagating perpendicularly to the magnetic field. For such waves, the particles are rendered stochastic by the presence of non-linear resonances. Karney[6] also showed, as a function of propagation angle, when the non-linear resonances must be considered.

The theories mentioned above are non-self-consistent in that the simultaneous effect of changes in the plasma particle distributions on the waves is not considered (except that a damping rate is provided). Although progress is being made in the construction of a self-consistent theory[7-8], very few experiments have been performed to test the validity of the non-self-consistent theories.[9-10]

This paper reports the results of experiments, in both an argon gas discharge and a barium Q-machine plasma, where the conditions

necessary for stochastic ion motion are created by excitation of electrostatic ion cyclotron waves and neutralized ion Bernstein waves. Both the linear and non-linear response of the plasma ions is detected using laser induced florescence (LIF). In addition to electric probes, the linear dielectric response provides information on the waves.[11] Observing the threshold for stochastic ion motion, the effect on the ion distribution function, and the time development of these changes provide several points of agreement with the non-self-consistent theories. Above threshold, however, evidence exists for self-consistent effects.

2. EXPERIMENTAL SET-UP

Two different plasmas have been used for these experiments. The first is an argon gas-discharge plasma with $n_e \sim 10^{11}$ cm^{-3}, $T_e \sim 14$ eV, $T_i \sim .3$ eV, a radius of 5 cm, and a length of 500 cm. A steady, uniform (± .3%) magnetic field $B \leq 3$ kG is used to radially confine the plasma.[12] Plasma is alternatively produced by a barium Q-machine source in the same vacuum vessel. The barium plasma has $n_e \leq 10^{10}$ cm^{-3}, $T_e \sim .2$ eV, $T_i \sim .2$ eV, and $T_{i\parallel} \sim .08$ eV.

An end-on view of the experimental set-up is shown in Fig. 1. The ion distribution function is measured from the spectrum of Doppler shifts during LIF.[13] In the argon plasma, a metastable state is used which is populated by the cathode electrons (see Fig. 1). In barium it is possible to pump directly the ionic ground state with visible light ($6^2S_{1/2} - 6^2P_{1/2}$, $\lambda = 4934$ Å) with the observed light being from the same transition. The laser bandwidth, which limits the measurement of Doppler shifts and therefore particle velocities, is $\Delta\nu \sim 600$ MHz. Pulses of 10 ns at a rate of 3 Hz are typical. Because the laser can be accurately triggered (jitter < 1 μsec), coherent oscillations of the distribution function can be observed. By orienting the laser beam and viewing volume at right angles, the distribution function measurements are made at a well-defined region in space (~ 50 mm^3). Particle velocities parallel to the laser beam are discriminated by tuning the laser wavelength. The vertical chord, on which the laser scans, can be freely scanned across the plasma column.

Electrostatic waves are generated by means of capacitor plate antennas which produce oscillations in the charge density at the plasma surface. As a check, the dispersion of the electrostatic waves, at low power, was compared with linear theory.[14] Figure 2 shows the observed dispersion relation in barium plasma compared to the roots of the expression

$$\epsilon = k_\perp^2 + k_\parallel^2 + \sum_{s=e,i} k_{DS}^2 \sum_{n=-\infty}^{\infty} [1+\zeta_{os} Z(\zeta_{ns})] e^{-\lambda_s} I_n(\lambda_s) = 0 \qquad (1)$$

where

$$k_{DS}^2 = \left(\frac{4\pi N q^2}{m v_t^2}\right)_s, \quad \lambda_s = \left[\frac{k_\perp v_{ts}}{\Omega_{cs}}\right]^2, \text{ and } \xi_{ns} = \frac{\omega - n\Omega_{cs}}{\sqrt{2} k_\parallel v_{ts}} .$$

Z is the plasma dispersion function and I_n is the modified Bessel function.

Examination of the dispersion relation for the parameter range of interest $\zeta_{oe} \ll 1$, $\zeta_{oi} \gg 1$ reveals the existence of two perpendicular wave numbers for a given choice of frequency and parallel wavenumber[15]:

- The electrostatic ion cyclotron wave (EICW).

$$\omega^2 \approx \left(k_\parallel^2 + \frac{\omega^2}{\omega^2 - \Omega_{ci}^2} k_\perp^2\right) C_s^2, \quad C_s^2 = \left(\frac{m_e v_{te}^2}{m_i}\right)$$

- The (neutralized) ion Bernstein wave (NIBW)

$$\sum_{n=1}^{\infty} I_n(\lambda_i) \frac{n^2}{(\omega/\Omega_{ci})^2 - n^2} = 0$$

In the gas-discharge $T_e/T_i \gg 1$ so that it is easy to avoid Landau damping over a range of wave parameters (frequency and parallel wavelength). In the barium plasma the region of parallel phase velocities which are slow enough to avoid electron Landau damping and yet fast enough to avoid ion Landau damping, is more restricted. In addition,

the dispersion curves for $T_e \sim T_i$ indicate propagating waves only over narrow bands of frequency. However, because $T_{i\parallel}$ is considerably lower than $T_{i\perp}$, the damping is reduced ($T_{e\parallel}/T_{i\parallel} \sim 3$). In both plasmas, the level of collisions is low enough not to produce significant damping. Because the Q-plasma has a rapid drift ($v_D \sim 10^5$ cm/sec) parallel to the magnetic field, the dispersion relation, in the laboratory frame of reference, is shifted in frequency by $-k_\parallel v_D$. Plasma ion drift is easily detected by doing LIF with the laser parallel to the magnetic field (Fig. 3).

A further check of linear theory involves measuring the perturbed distribution function. The laser observes a distribution function which has been integrated over the velocity components transverse to the laser beam. If the laser is normal to both the magnetic field and the wave vector one has from linear theory[11]

$$f_i^{(1)}(v_y,xt) = \frac{-q\Phi(x,t)}{m_i v_{ti}^2} \sum_{n,m=-\infty}^{\infty} J_m(a) I_n\left(\frac{\lambda}{4}\right) e^{\frac{\lambda}{4}+ia-im\frac{\pi}{2}} \zeta_o Z(\zeta)_{2n+m} f^{(0)}(v_y) \qquad (2)$$

$$a \equiv k_\perp v_y/\Omega_{ci}$$

Figure 4 shows a comparison with theory of the perturbed distribution function in barium plasma with waves being generated at a single frequency $\omega/\Omega_{ci} = 2.15$ (in the plasma frame). The response is complicated by the presence of the two perpendicular wave-numbers for a given frequency.

Though it is very difficult to find evidence of the NIBW from electric probe data, the short "wavelength" oscillation of f^1 as a function of v_y are easily evident in Fig. 4. Figure 5 shows the result of the parameter fit in Fig. 4. Since the dielectric response is linear in wave amplitude, it can be used to determine the wave potential. Figure 6 shows the measured relationship between the first moment of f^1, that is the average velocity $\langle v_y \rangle = \int f^1 \cdot v_y \, dv_y$, and the antenna current. In this way, the laser can be used to determine the amplitude, wave vector, and phase of the electrostatic waves.

3. OBSERVATIONS NEAR THRESHOLD

Dielectric response represents a reversible action on the distribution function. Above a certain level of wave amplitude, however, rapid changes are observed in the ion distribution function which remain, even if the wave generation is stopped (although they decay on an particle confinement timescale).

The threshold fields for overlap of the two kinds of resonance are given in Table 1.

		Wave
Ref. 5-6	$\frac{E_\perp}{B_o} \sim \frac{1}{4}\left(\frac{\Omega_{ci}}{\omega}\right)^{1/3} \cdot \frac{\omega}{k_\perp c}$	NIBW
Ref. 3	$\frac{E_\parallel}{B_o} \sim .3\,\frac{\Omega_{ci}}{\omega} \cdot \frac{\omega}{k_\parallel c}$	EICW

Table 1

Since the NIBW and EICW are observed to be excited with a similar value of electric field, stochasticity due to the NIBW (according to the mechanism described by Karney) has the lowest threshold in terms of antenna current. Since the NIBW has a phase velocity near the ion thermal velocity, interaction is with the "bulk" of the distribution and it remains roughly maxwellian.[6] Figure 7(a) demonstrates the relatively sudden change of the argon ion temperature as a function of rf antenna current. The changes are also rapid, requiring only a few gyro-periods (Fig. 7(b)), as is typical for stochastic motion.[3,6] Figure 8 shows the corresponding changes in the distribution function. In the barium plasma, where there were also measurements of $f(v_\parallel)$, changes in the distribution function were observed first perpendicular to the field and (at higher power) parallel to the field (Fig. 9). It is better to think in terms of modifications of the distribution functions rather than simply of changes in temperature, especially concerning the parallel distribution which is broadened only in the direction of wave propagation.

The change in the parallel distribution function at high power occurs at the field level associated with the overlap of cyclotron resonances. Figure 10 shows calculated Poincaré section plots of ion orbits using the Hamiltonian of Smith and Kaufman[3]

$$H(z,\phi,P_z,P_\phi) = P_z^2/2m_i + P_\phi\Omega_{ci} + e\Phi_o \sin(k_\parallel z - k_\perp\rho_i \sin\phi)$$

with the EICW wave vector $k_\perp/k_\parallel = 10$. For $\varepsilon \equiv k_\parallel^2 e\Phi_o/m\Omega^2 \sim .3$ both theory and experiment demonstrate ion acceleration parallel to the magnetic field.

Several points of agreement exist, therefore, between these experiments and the predictions of non-selfconsistent stochasticity theory. The threshold, the time required, and the form of the resultant changes in the distribution function all seem to agree with single particle theory.

4. EVIDENCE FOR SELF-CONSISTENT EFFECTS

Self-consistent effects are observed in at least two instances in these experiments. First it should be said that linear wave theory appears to hold throughout. There is no evidence of parametric or parasitic waves due to changes in the ion distribution (although the electrons show some activity at high wave power) and the linear dielectric response is still visible on top of the secular changes of the distribution function.

Because the wave vector, particularly of the NIBW, is sensitive to ion temperature, the perpendicular wavelength is observed to change (increase) with increased ion temperature. Therefore (Table 1) the threshold increases with ion temperature which may tend to saturate the process as observed in Fig. 7(a). Wave coupling may also change with changes in the distribution function. A futher complication occurs when the parallel distribution is broadened. Given the heated distribution, the waves should continue to be strongly (linearly Landau) damped even after they have decayed to a level below the threshold.

A second point which is nearly visible in Fig. 7(b), but more striking for higher wave fields (Fig. 11(a)), is the transient time behaviour of the particle distribution and waves when the waves are first launched. Figure 11(a) shows the time evolution of the ion temperature (for lack of a better parameter) as a function of time after the waves have been engaged. An indication of the influence on the waves is given by the dielectric response $\langle v_y \rangle$ (Fig. 11(b)). The relation of these transients to the amplitude oscillations observed in initial-value self-consistent calculations[8] is not yet known.

5. SUMMARY

Many experiments remain to be done concerning wave particle interactions. We have presented experiments involving waves near the stochasticity threshold. Non-self-consistent theories predict correctly the threshold level of wave amplitude for rapid changes in the ion distribution fucntion. The form of the distortion of the distribution function is also very similar to the results of these calculations. On closer examination, however, there exist a number of elements in these experiments which require the inclusion of self-consistent effects.

ACKNOWLEDGEMENTS

This work was partially funded by the Swiss National Science Foundation under grants Nos 2.868-0.85 and 2.869-0.85, and by the US National Science Foundation under grant No INT-840.5076. The Q-device source was partially developed at the University of California at Irvine under the U.S. National Science Foundation grant No Phy-860.6081. The authors would like to acknowledge the technical support of Messrs. A. Gorgerat and A. Simik and of the whole staff of the Centre de Recherches en Physique des Plasmas.

REFERENCES

1 G.M. Zaslavskii and B.V. Chirikov, Sov. Phys. Uspekki 14, (1972) 549.
B.V. Chirikov, CERN Report 267, Oct. 1971.

2 D.F. Escande, Phys. Rep. 121, Nos 3 & 4, (1985) 166.

3 G.R. Smith and A.N. Kaufman, Phys. Rev. Lett. 34, (1975) 1613.

4 A. Fukuyama, H. Momota, R. Itatani and T. Takizuka, Phys. Rev. Lett. 38, (1977) 701.

5 C.F.F. Karney and A. Bers, Phys. Rev. Lett. 39, (1977) 550.

6 C.F.F. Karney, Phys. Fluids 21, (1978) 1584 and Phys. Fluids 22, (1979) 2188.

7 J.A. Krommes, Princeton Plasma Physics Laboratory Report, PPPL-AF-89 (1979).

8 C.R. Menyuk, Phys. Fluids 26, (1983) 705.

9 F. Doveil, Phys. Rev. Lett. 46, (1981) 532.

10 F. Skiff, F. Anderegg and M.Q. Tran, Phys. Rev. Lett. 58, (1987) 1430.

11 F. Skiff and F. Anderegg, submitted to Phys. Rev. Lett.

12 M.Q. Tran, P. Kohler, P.J. Paris and M.L. Sawley, Centre de Recherches en Physique des Plasmas Report LRP 205/82 (1982).
P. Kohler, R.A. Stern, B.A. Hammel, M.Q. Tran, B.M. Lamb, P.J. Paris and M.L. Sawley, Proceedings of Contributed Papers, 1984 International Conference on Plasma Physics, Lausanne, edited by M.Q. Tran and M.L. Sawley, Vol. 2, p.317.

13 R.A. Stern and J.A. Johnson III, Phys. Rev. Lett. 34 (1975) 1548.
F. Anderegg, R.A. Stern, F. Skiff, B.A. Hammel, M.Q. Tran, P.J. Paris and P. Kohler, Phys. Rev. Lett. 57 (1986) 329.

14 F. Skiff, F. Anderegg, M.Q. Tran, P.J. Paris, T. Good, R.A. Stern and N. Rynn, Contributed Paper: "Finite Amplitude Electrostatic Waves", 1987 International Conference on Plasma Physics, Kiev, USSR.

15 J.P.M. Schmidt, Phys. Rev. Lett. 31, (1973) 982.

FIGURE CAPTIONS

Fig. 1 Experimental set-up. In the barium plasma the laser was also able to probe in the direction parallel to the magnetic field.

Fig. 2 Linear dispersion relation in the barium plasma. The corresponding data for the argon plasma are in Ref. 14.

Fig. 3 Line position in perpendicular and parallel LIF. Doppler shift indicates ion drift.

Fig. 4 (a) Measured perturbed distribution function in the presence of waves.

(b) Prediction of Eq. (2) constrained by (1) including the influence of both the NIBW and EICW. Free parameters are the amplitude and phase of each wave.

Fig. 5 Laser measurement of wave dispersion if the values of $k_{\parallel}$ (rather than being constrained by Eq. (1)) are fit to the data, they also agree with the dispersion relation.

Fig. 6 Relation between antenna r.f. current and the dielectric velocity transverse to the wave $\langle v_y \rangle$.

Fig. 7 (a) Argon ion temperature as a function of antenna current.

(b) Time evolution of the ion temperature with a pulsed r.f. signal ($\omega/\Omega_{ci} = 3.5$).

Fig. 8 Argon ion distribution function below and above the threshold ($\omega/\Omega_{ci} = 3.5$).

Fig. 9 Barium ion distribution functions a) $f(v_y)$ b) $f(v_{\parallel})$ as a function of wave amplitude. $\varepsilon=0$, $I_{rf}=1A$ ($\varepsilon=.2$), $I_{rf}=1.5A$ ($\varepsilon=.3$). ε is defined as $k_{\parallel}^2 e\Phi_o/m\Omega_{ci}^2$, where Φ_o is the wave potential ($\omega/\Omega_{ci} = 2.15$).

Fig. 10 Poincaré section plots P_z-Z and P_z-ρ for a), b) $\varepsilon=.003$; c)d) $\varepsilon=.16$; e)f) $\varepsilon=.3$.

Fig. 11 (a) Time development of barium ion temperature T_i for pulsed r.f. above threshold.

(b) Time development of the dielectric velocity $\langle v_y \rangle$.

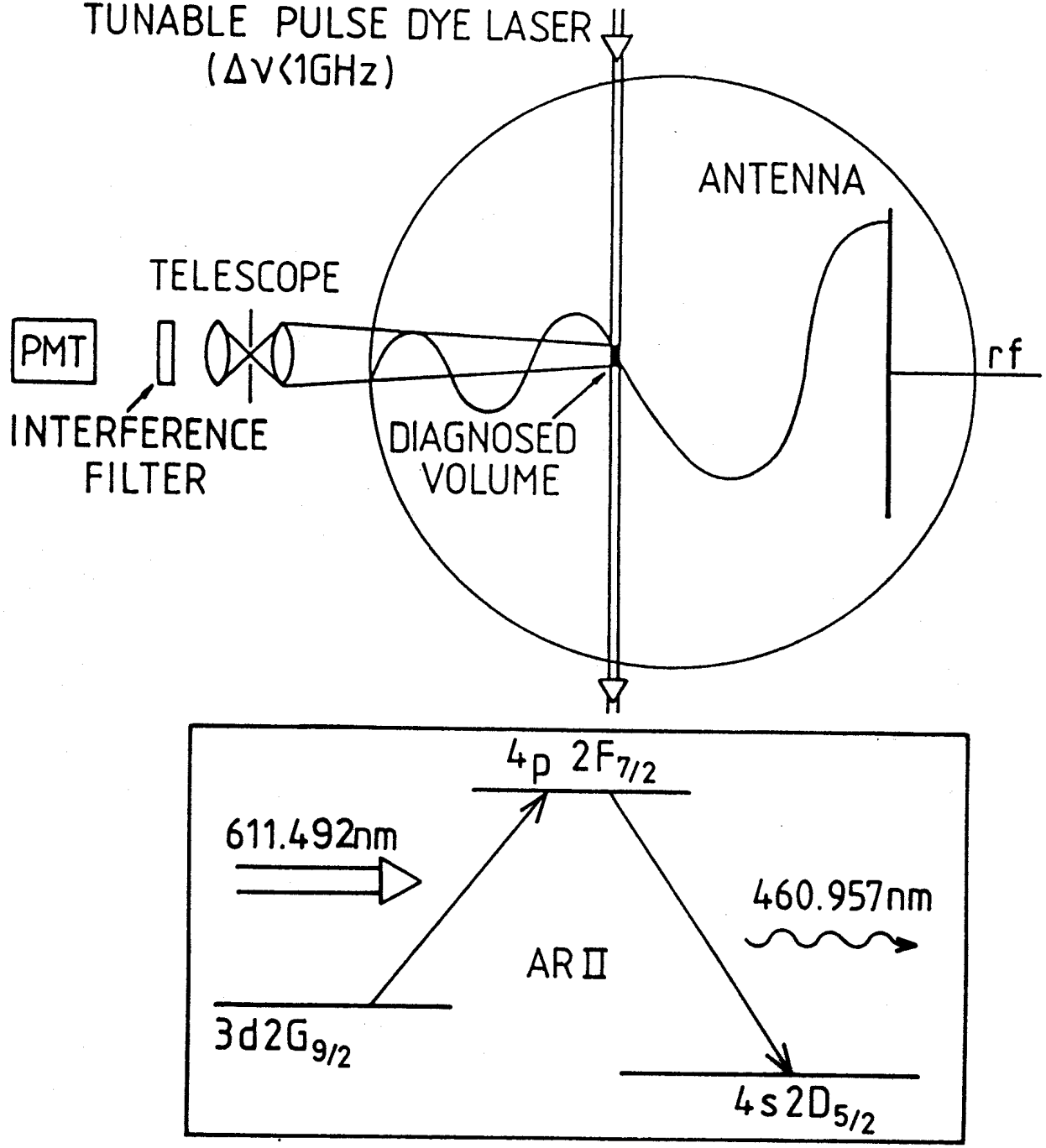
TUNABLE PULSE DYE LASER
(Δν<1GHz)
ANTENNA
TELESCOPE
PMT
rf
INTERFERENCE
FILTER
DIAGNOSED
VOLUME
4p 2F7/2
611.492nm
460.957nm
AR II
3d2G9/2
4s2D5/2

FIG. 1

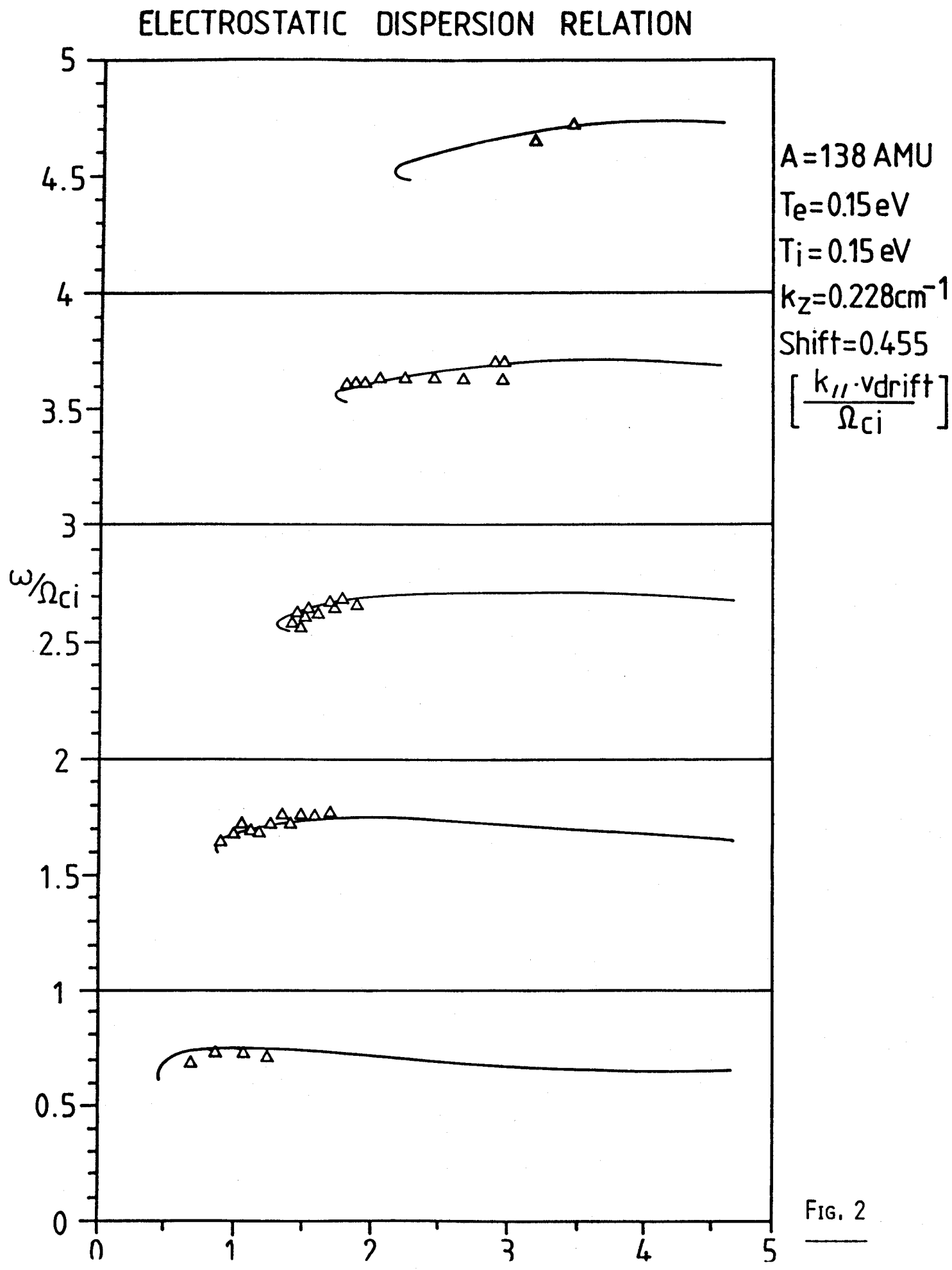
ELECTROSTATIC DISPERSION RELATION
A=138 AMU
Te=0.15 eV
Ti=0.15 eV
kz=0.228cm-1
Shift=0.455
[k// · vdrift / Ωci]
ω/Ωci
0
0.5
1
1.5
2
2.5
3
3.5
4
4.5
5
0
1
2
3
4
5

FIG. 2

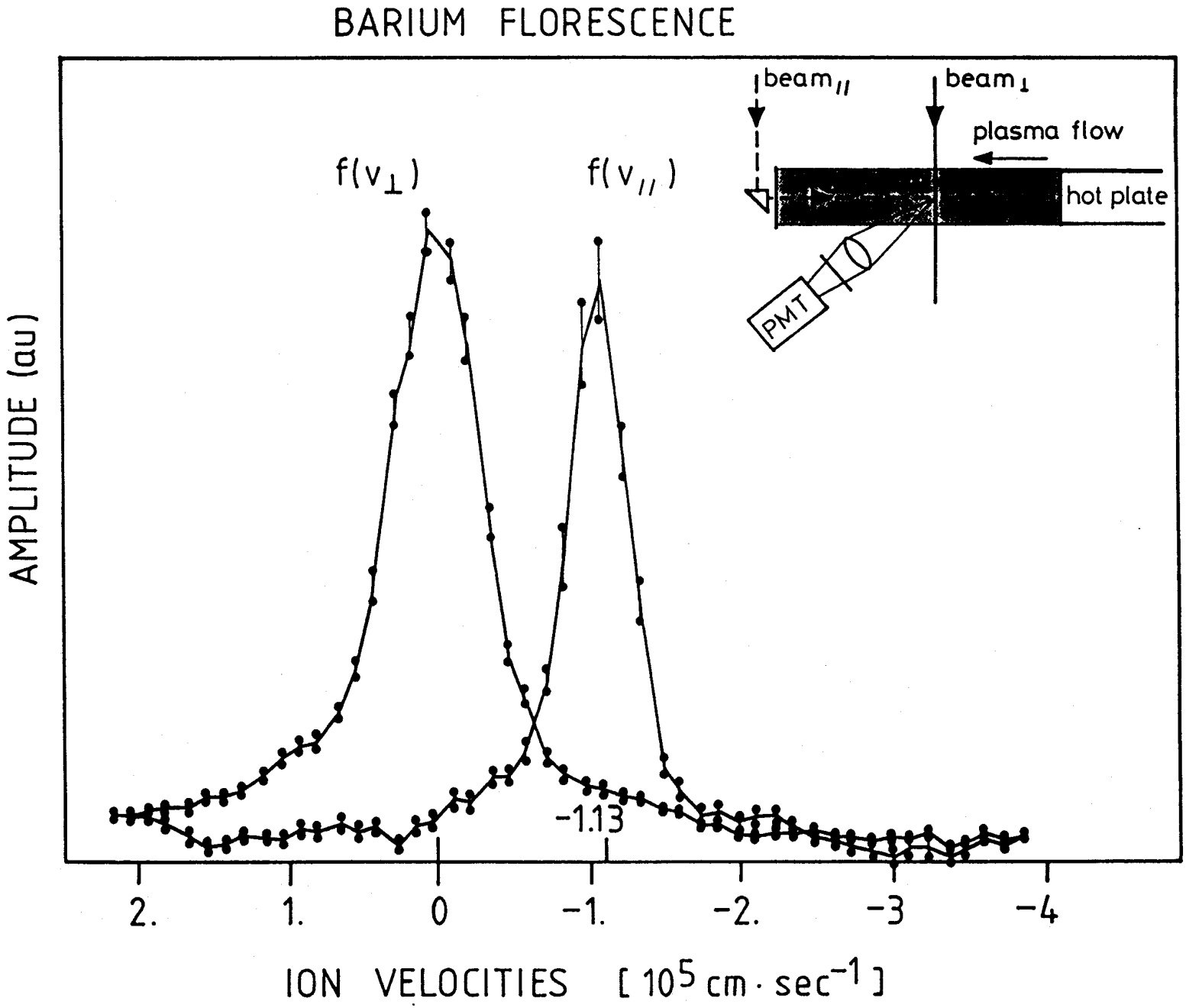
BARIUM FLORESCENCE
beam//
beam⊥
plasma flow
hot plate
PMT
f(v⊥)
f(v//)
-1.13
AMPLITUDE (au)
2.
1.
0
-1.
-2.
-3
-4
ION VELOCITIES [10^5 cm · sec^-1]

FIG. 3

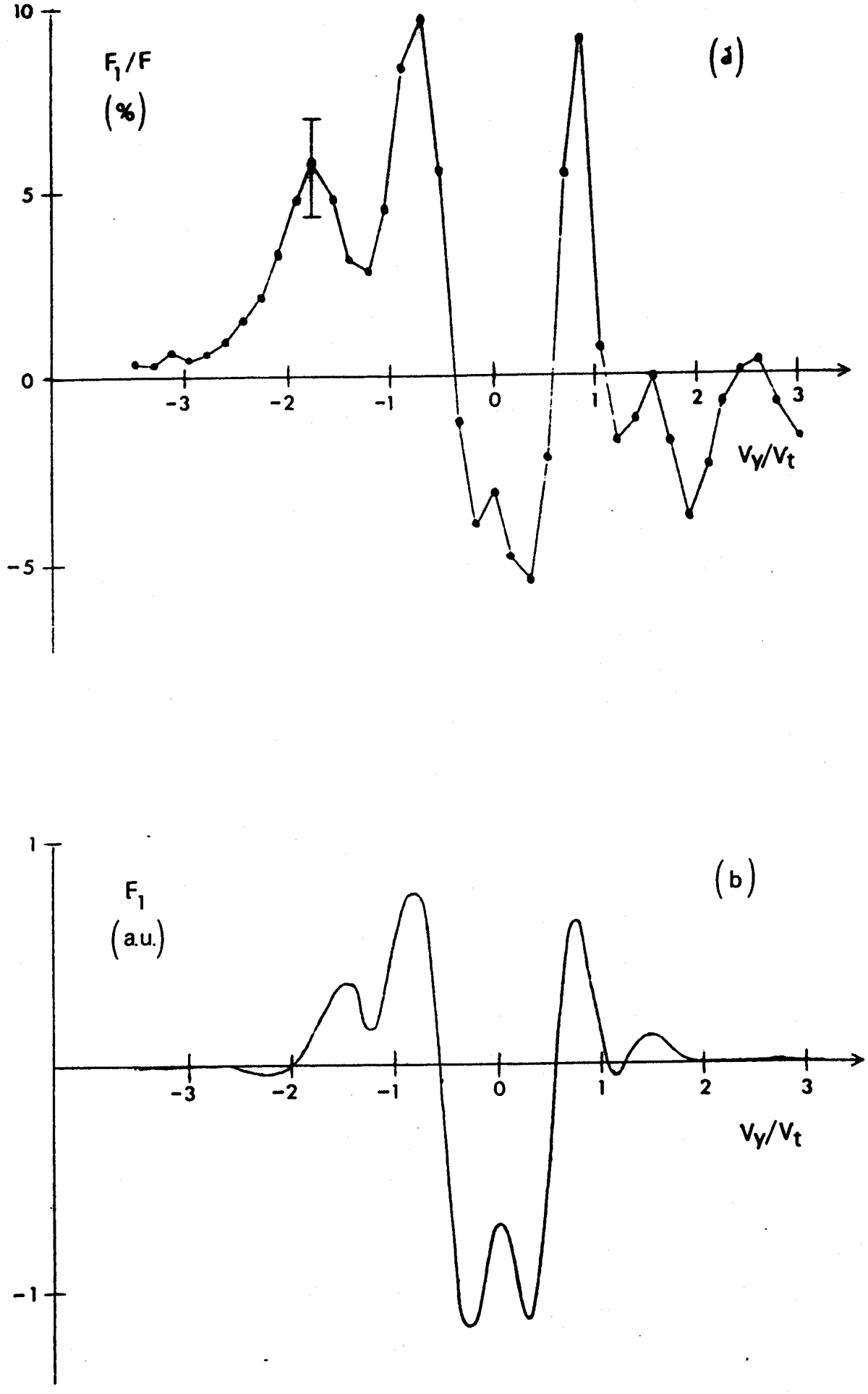

FIG. 4

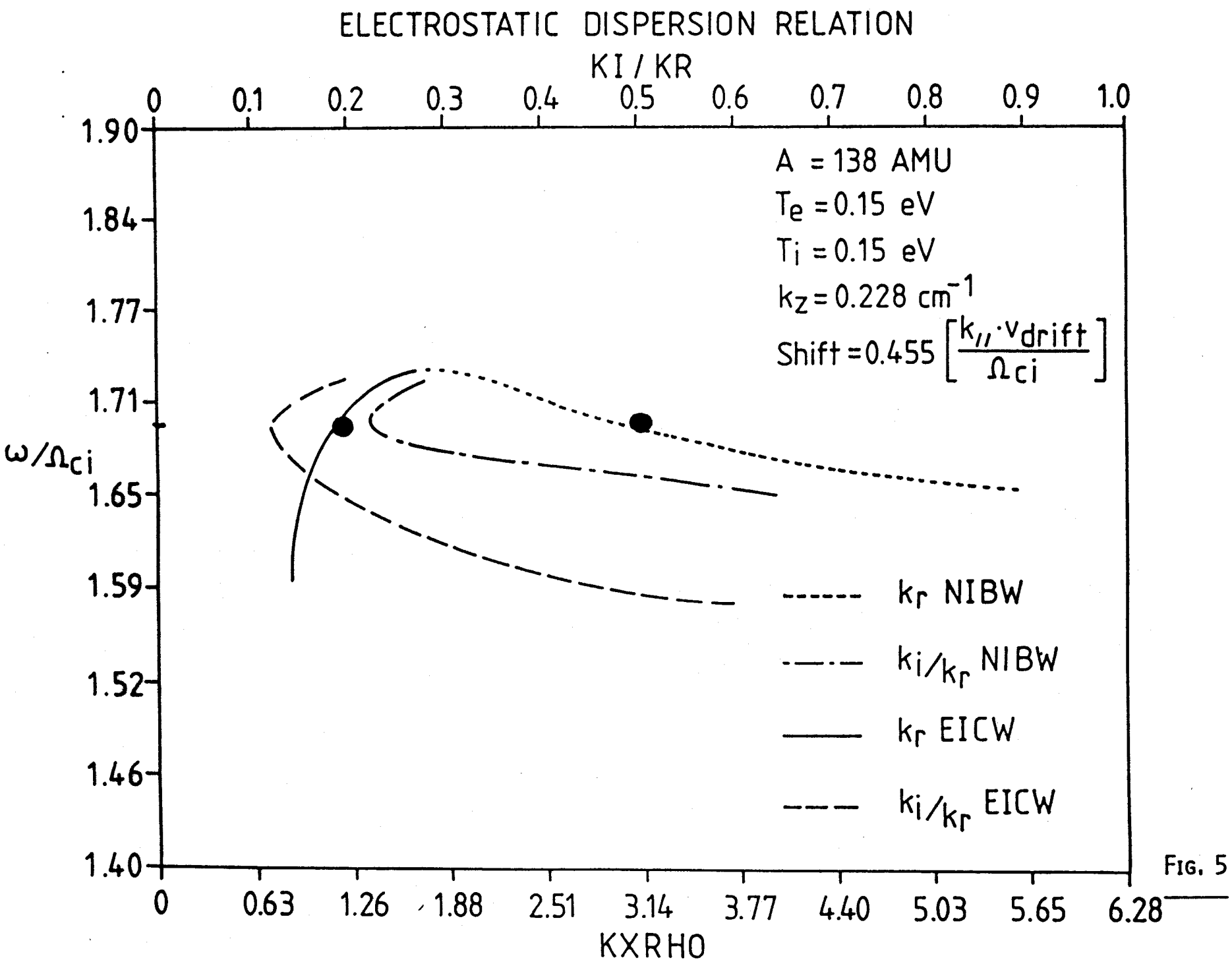
ELECTROSTATIC DISPERSION RELATION
KI / KR
0
0.1
0.2
0.3
0.4
0.5
0.6
0.7
0.8
0.9
1.0
1.90
1.84
1.77
1.71
1.65
1.59
1.52
1.46
1.40
ω/Ωci
A = 138 AMU
Te = 0.15 eV
Ti = 0.15 eV
kz = 0.228 cm⁻¹
Shift = 0.455 [k// · vdrift / Ωci]
kr NIBW
ki/kr NIBW
kr EICW
ki/kr EICW
0
0.63
1.26
1.88
2.51
3.14
3.77
4.40
5.03
5.65
6.28
KXRHO

FIG. 5

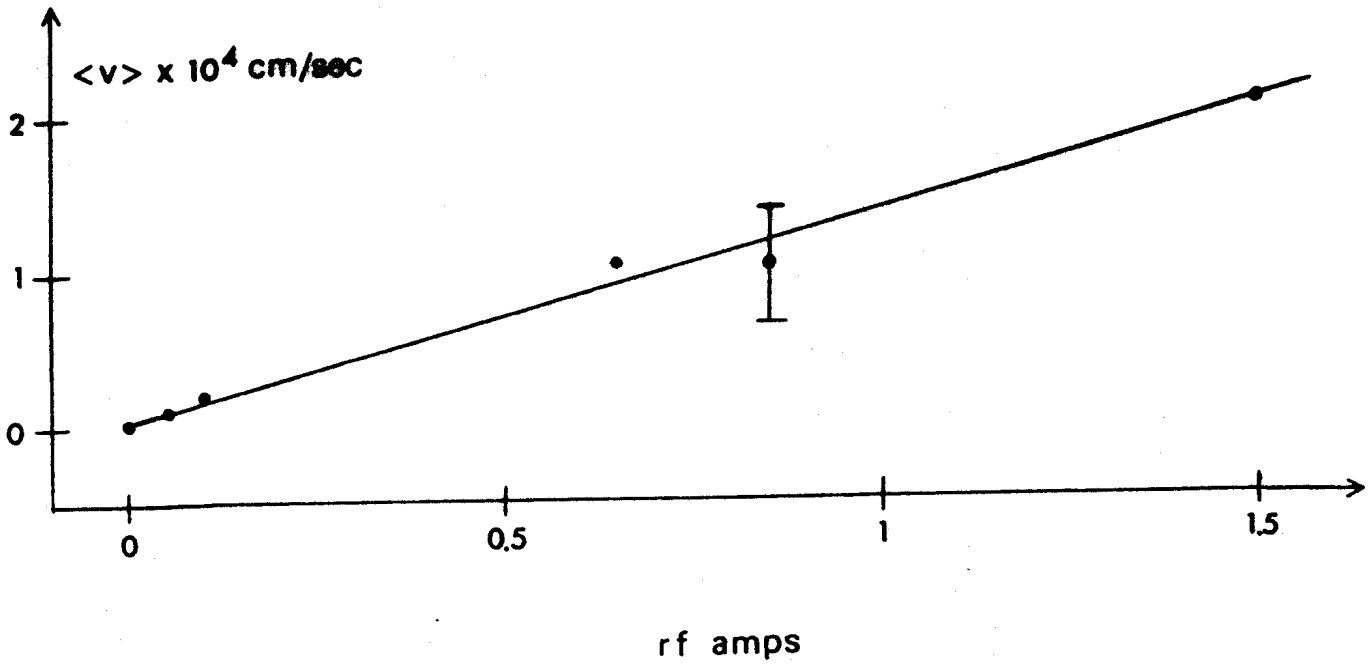

FIG. 6

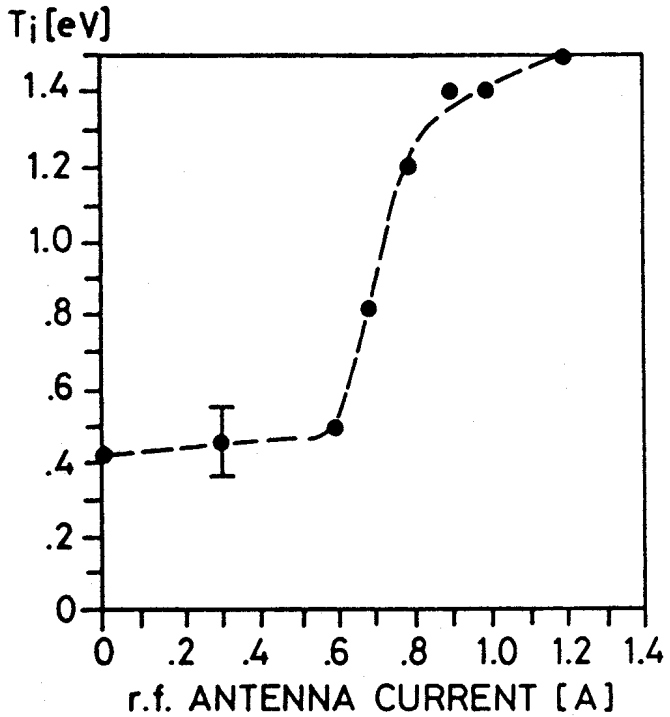
T_i [eV]
1.4
1.2
1.0
.8
.6
.4
.2
0
0 .2 .4 .6 .8 1.0 1.2 1.4
r.f. ANTENNA CURRENT [A]

FIG. 7 A)

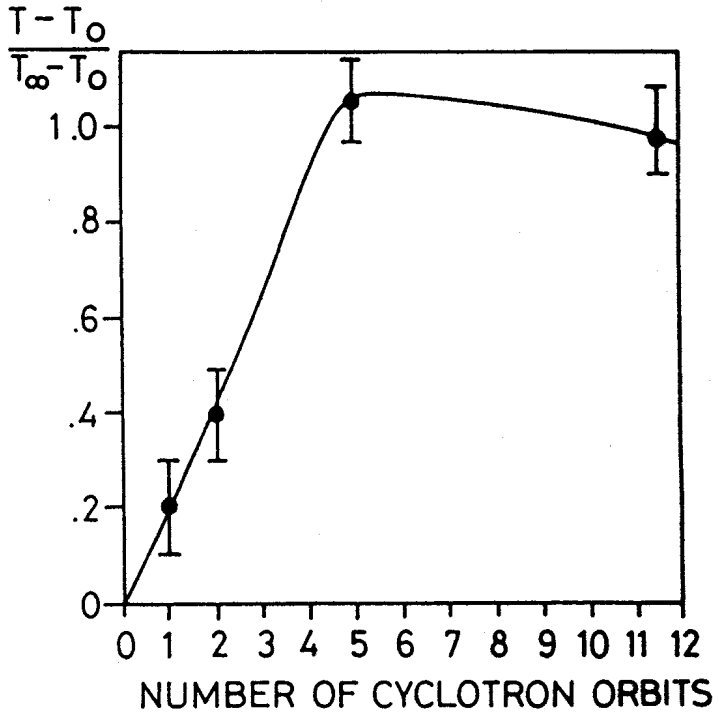
$\frac{T-T_o}{T_\infty-T_o}$
1.0
.8
.6
.4
.2
0
0 1 2 3 4 5 6 7 8 9 10 11 12
NUMBER OF CYCLOTRON ORBITS

FIG. 7B)

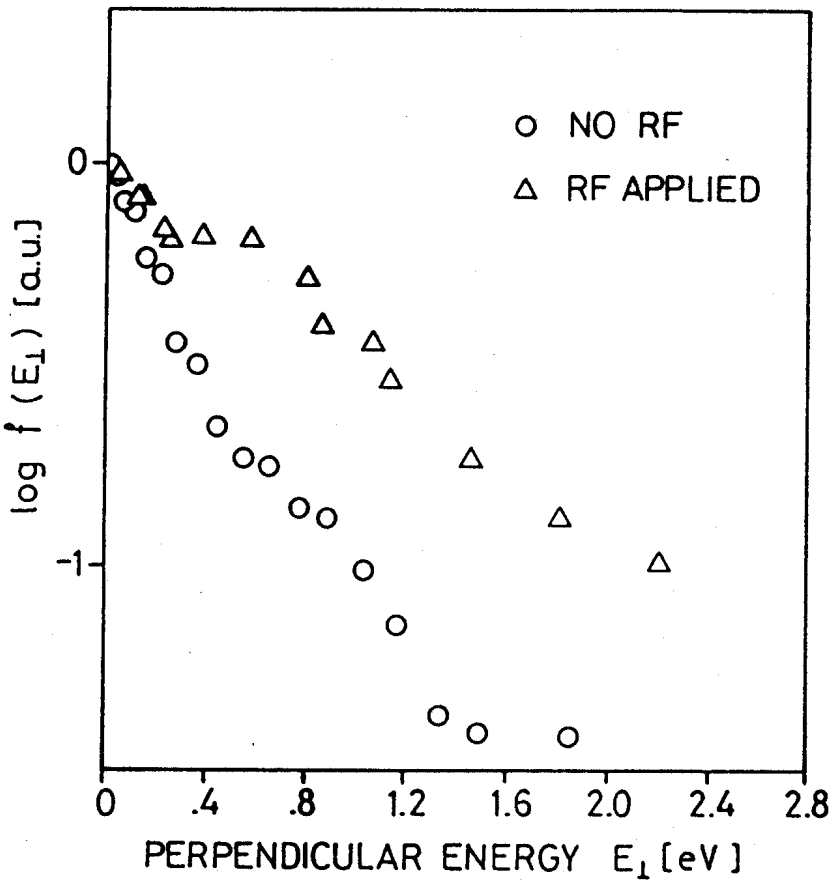
NO RF
RF APPLIED
0
-1
log f (E⊥) [a.u.]
0
.4
.8
1.2
1.6
2.0
2.4
2.8
PERPENDICULAR ENERGY E⊥ [eV]

FIG. 8

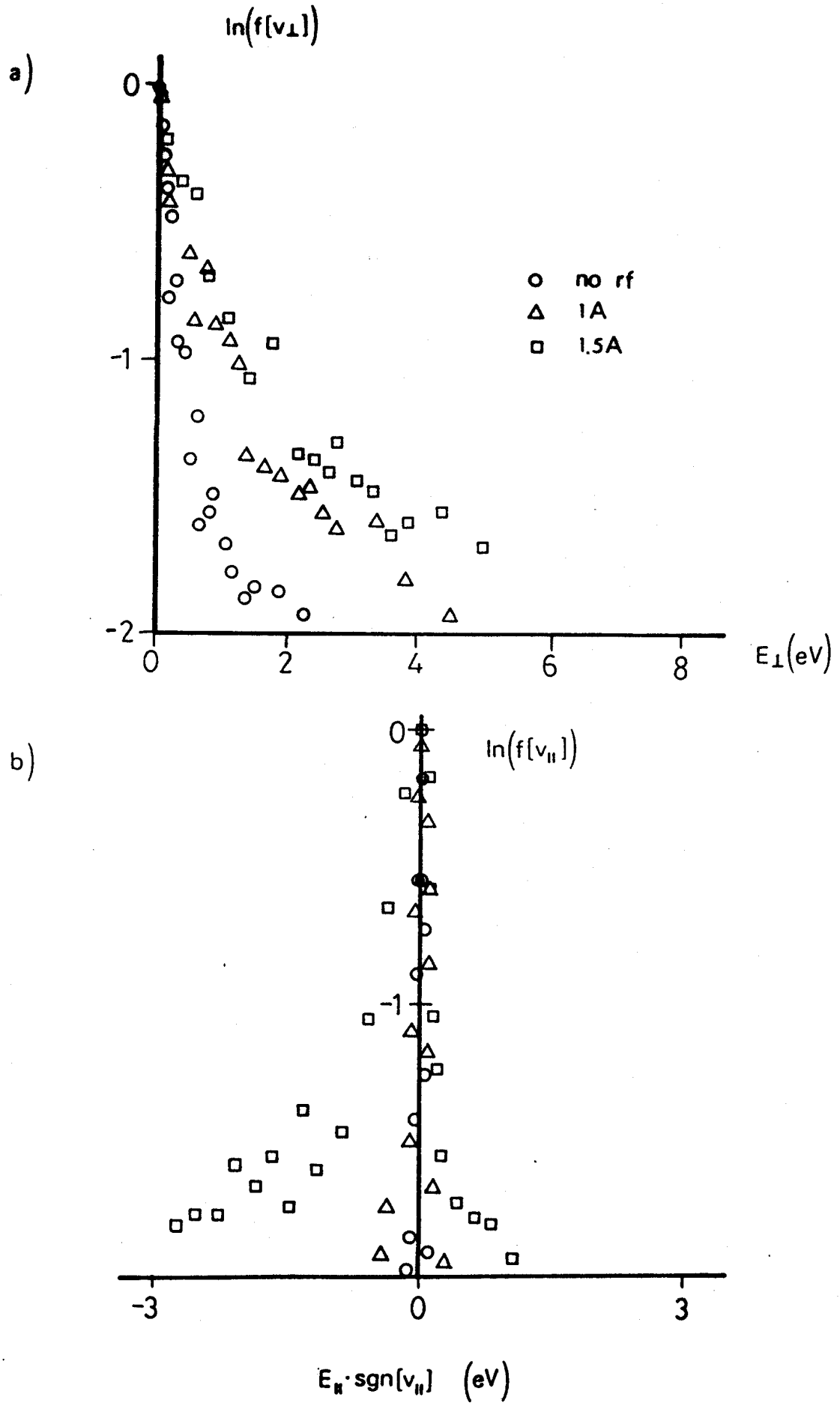

FIG. 9

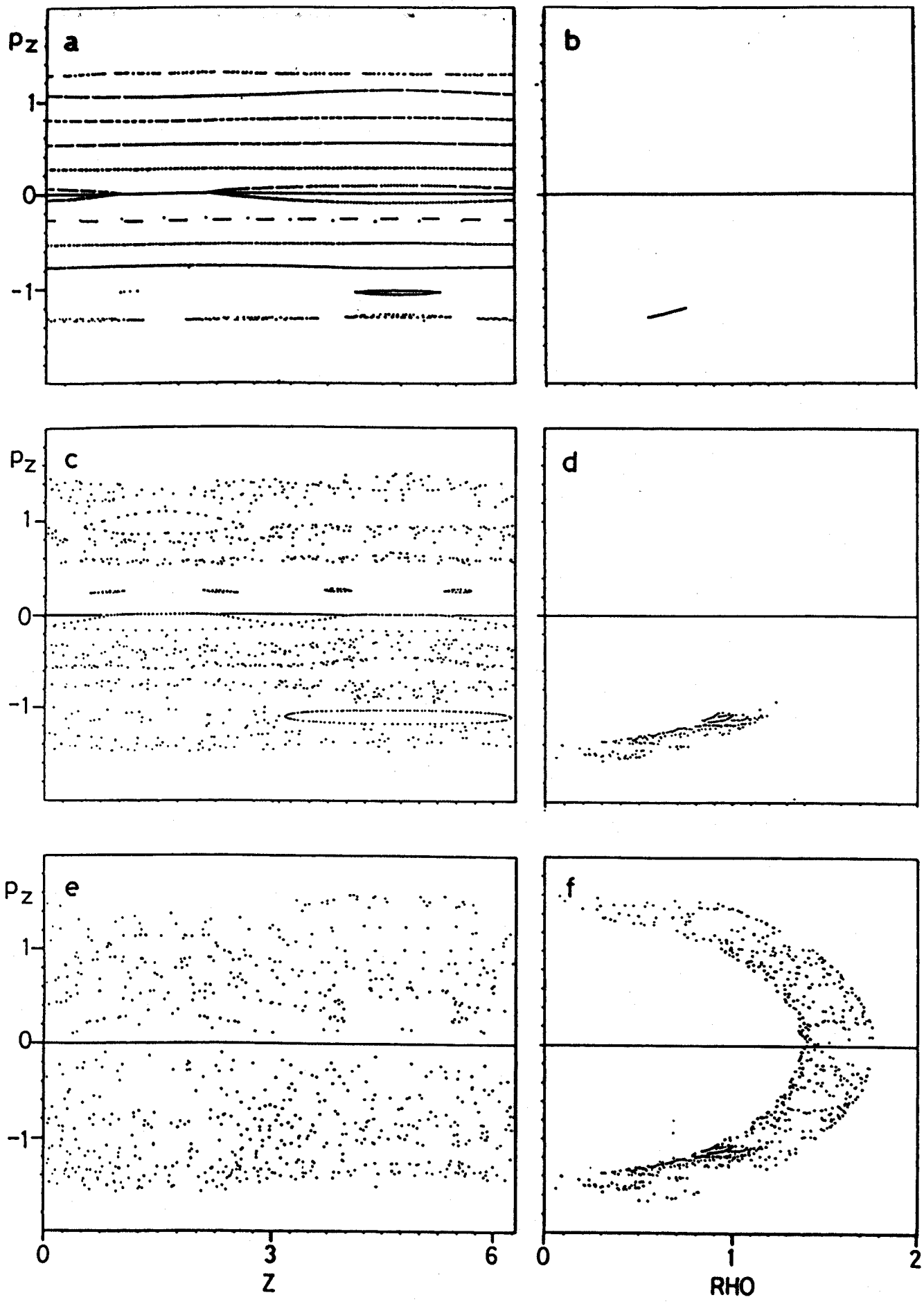

FIG. 10

FIG. 11

a)

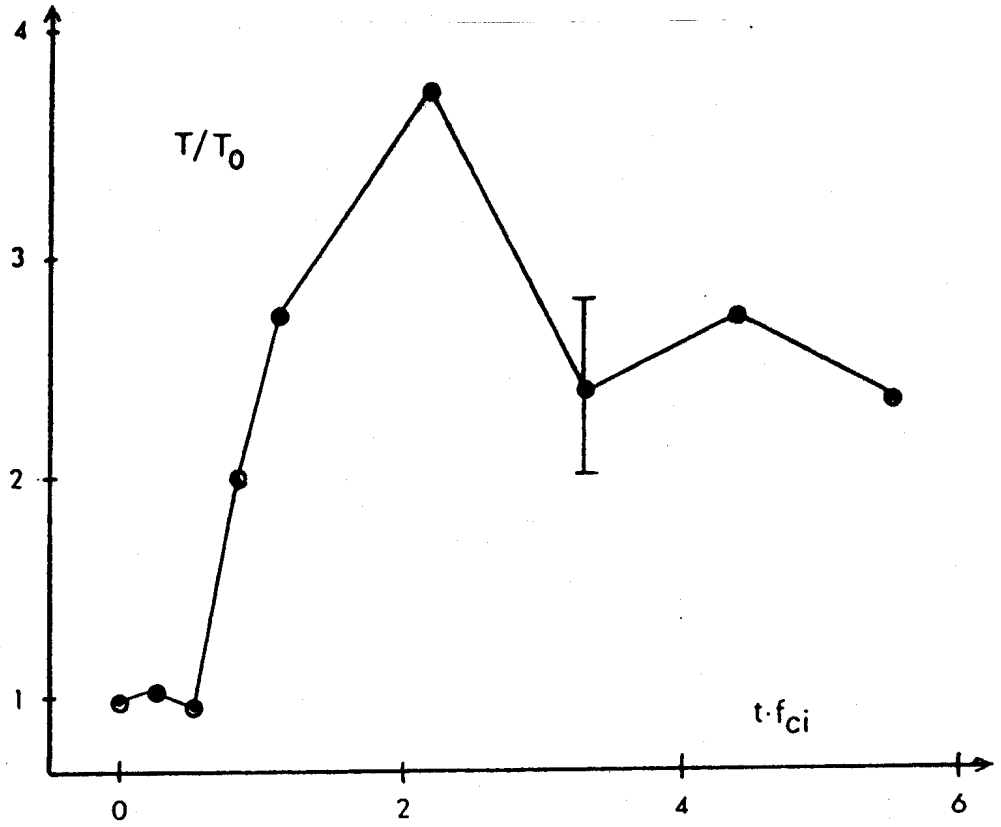

b)

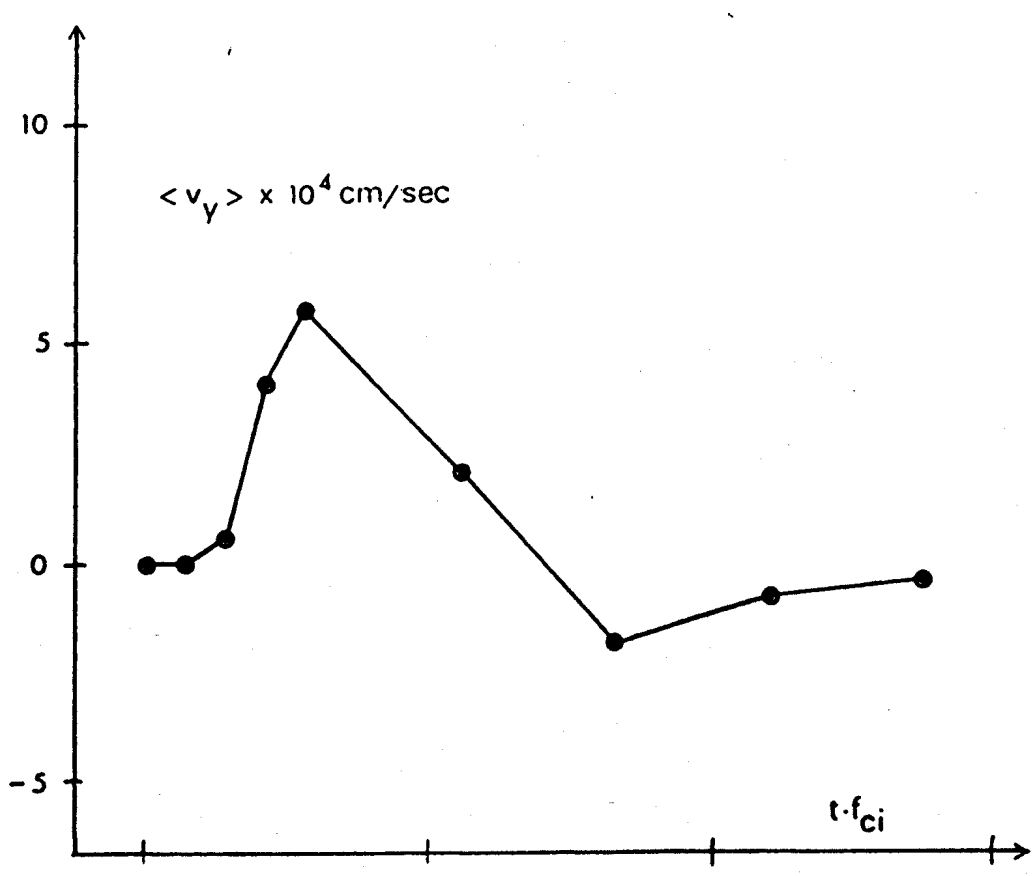

CONTRIBUTED PAPERS

FINITE AMPLITUDE ELECTROSTATIC WAVES

F. Skiff, F. Anderegg, M.Q. Tran, P.J Paris, T. Good,
R.A. Stern and N. Rynn

EVOLUTION OF ELECTROSTATIC WAVES AND BEAM DISTRIBUTION FUNCTION IN A BEAM PLASMA SYSTEM

J.A. Michel, J.-P. Hogge, P.-J. Paris, A. Frey and M.Q. Tran

FINITE AMPLITUDE ELECTROSTATIC WAVES

F. Skiff, F. Anderegg, M.Q. Tran, P.J Paris, T. Good,
R.A. Stern[+] and N. Rynn[*]

Centre de Recherches en Physique des Plasmas
Association Euratom - Confédération Suisse
Ecole Polytechnique Fédérale de Lausanne
21, Av. des Bains, CH-1007 Lausanne/Switzerland

Permanent address

+ Dept. of Astrogeophysics, University of Colorado at Boulder, Boulder, CO 80309, U.S.A.

* Dept. of Physics, University of California at Irvine, Irvine, CA 92717, USA

ABSTRACT

Wave physics in the ion-cyclotron frequency range is very rich in linear and non-linear phenomena. This situation is partly due to the multiplicity of wave types and the importance of wave-particle interactions. Here we consider the linear hot plasma electrostatic response of a cylindrical gas-discharge plasma. Electric probes are used to measure wave potential and laser induced florescence [1] is used to observe the plasma dielectric response.

The dispersion relation for electrostatic waves in a magnetized hot plasma has principally two roots in the ion cyclotron frequency range. The electrostatic ion cyclotron (acoustic) wave

$$\omega^2 \approx (k_z^2 + \frac{\omega^2}{\omega^2-\Omega_i^2} k_r^2)c_s^2 \; ; \; c_s^2 = \frac{2KT_e}{m_i}$$

and the ion Bernstein wave

$$\sum_{n=1}^{\infty} I_n(\Lambda_i) \frac{n^2}{(\omega/\Omega_i)^2-n^2} \approx 0$$

The dispersion relation is shown in Fig. 1 along with data from a gas-discharge with $T_e \sim 14$ eV, $T_i \sim .1$ eV, $n \sim 10^{11} cm^{-3}$ and $B_o = 2$ kG. Solid curves represent the dispersion relation, and dashed curves indicate the level of linear damping. The waves are launched by a series of plates at the plasma edge which couple capacitively to the plasma column [2]. The parallel wavelength is determined by the size and separation of the plates along the magnetic field.

To obtain a picture of the wave fields generated, one can start from the electrostatic wave equation $\nabla \cdot K \cdot \{E\} = 4\pi\rho_{free}$, where ρ_{free} represents the oscillating charge on the antennas, and K is the hot plasma dielectric tensor. Figure 2a shows a typical reconstructed waveform for $\omega/\Omega_{ci} \sim 3.5$, the two distinct wavelengths of the electrostatic ion-cyclotron wave (EICW) and the short wavelength neutralized ion Bernstein wave (NIBW) are evident. Figure 2b shows data from an experiment with the same parameters as were used in the simulation.

Laser induced florescence can be used to diagnose the influence of waves on the ion distribution function in a non-perturbative manor. The experimental set-up is shown in Fig. 3. A narrow band tunable (dye) laser is used to excite resonant transitions in the bulk plasma ionic states (Ar^+ here). Doppler broadening of the resonance absorption provides a measure of ion velocities along the laser beam axis. Florescence is observed along a chord at right angles to the

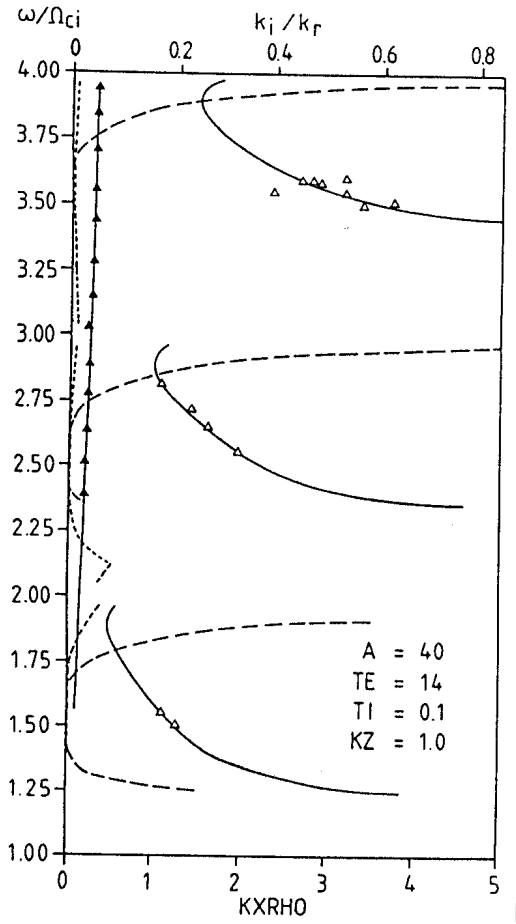

Fig. 1: Electrostatic dispersion relation. Triangles are data points.

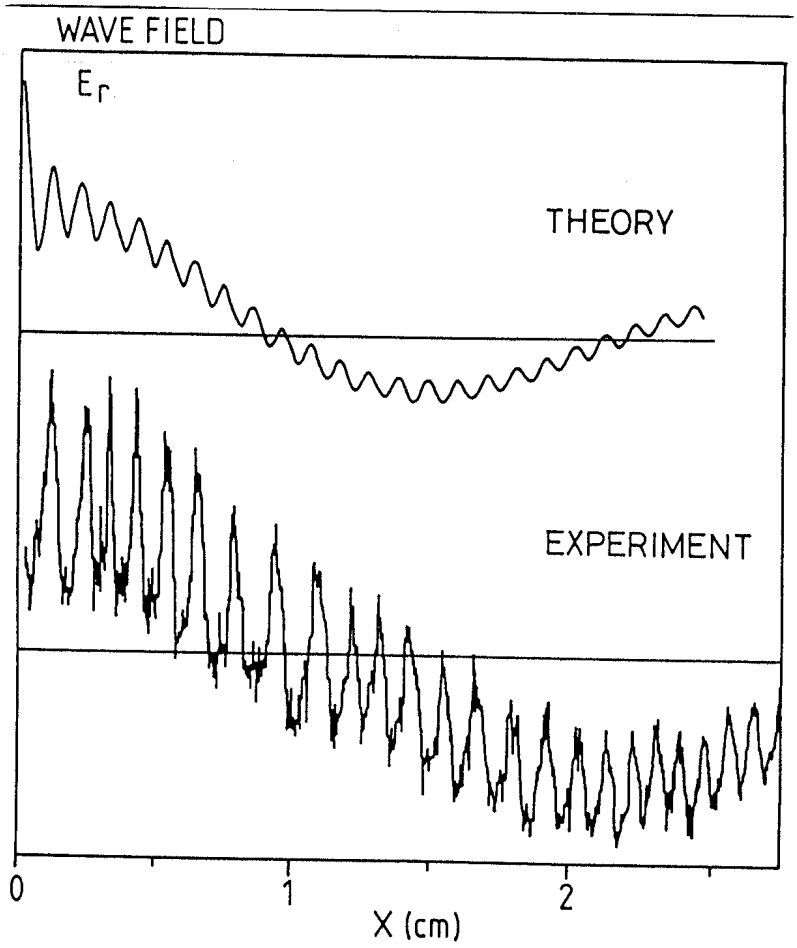

Fig. 2: Wave interferograms
a) reconstructed from wave equation
b) from probe data

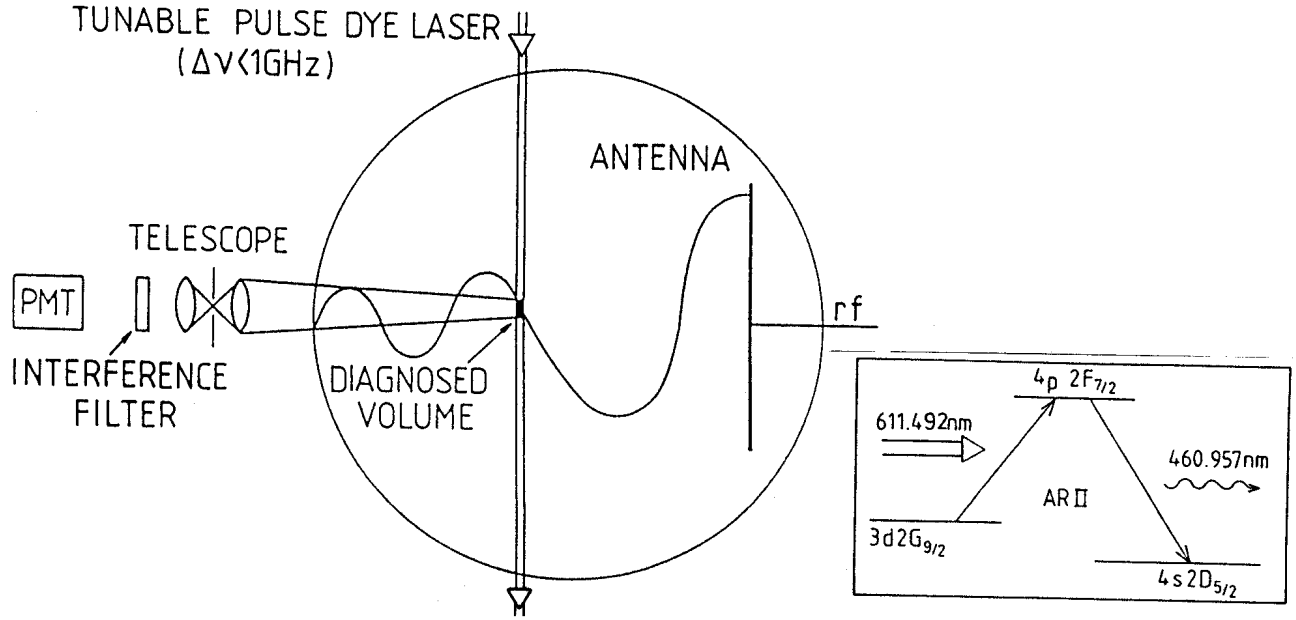

Fig. 3: Experimetnal set-up for LIF. Also shown are the ionic transitions used.

beam axis so that the diagnosed volume is very localized. Sub-microsecond time resolution is also possible (10 nsec laser pulse length).

The linear dielectric response of plasma ions can be represented in terms of a mobility $\underline{V} = \underline{M} \cdot \underline{E}$, where $\underline{E}$ is the self-consistent plasma electric field. By making measurements of ion velocities which are syncronous with the externally applied electric fields, the dielectric response of plasma ions, and therefore the internal plasma electric field can be determined. Figure 4a shows the measured (average) velocity transverse to a central chord, at several positions along this central chord. Figure 4b shows a reconstruction of the anticipated electric field pattern of the wave along a central chord for the same plasma parameters. In this case, the connection between wave field and

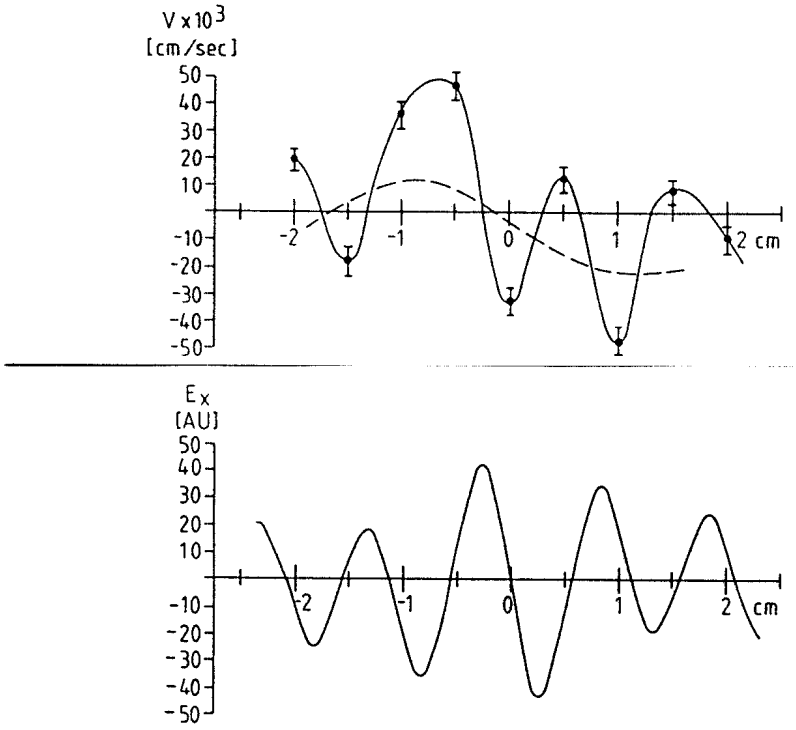

Fig. 4: Dielectric motion implies electric field

a) measured average transverse ion velocity synchronous with applied rf.

b) calculated electric field profile for the same conditions.

the average transverse ion velocity is given by $\langle V_g \rangle = M_{yx} E_x$

$$\langle V_y \rangle = \frac{E_x}{B_o} \frac{\Omega_{ci}}{k V_i} \sum_{n=1}^{\infty} n(I_n - I_n') e^{-\lambda} (Z_n - Z_{-n})$$

where $\lambda = (k v_i/\Omega_{ci})^2$ and Z_n is the plasma dispersion function with argument $\omega - n\Omega_{ci}/k_\parallel V_i$.

With synchronous laser measurements it is possible to go further than measuring the line shift to measure the dielectric motion of subgroups in velocity space. The different regions of velocity space may contribute differently to the dielectric motions. For example, NIBW dispersion characteristics are largely determined by a balance between the response of ions above and below the ion thermal velocity.

Experiments involving the observation of the spatial and velocity displacements of plasma ions with selectively populated (or depopulated) internal ionic levels promise to provide more detailed descriptions of plasma ion response in the presence of electrostatic waves.

References

1. R.A. STERN and I.A. JOHNSON III, Phys. Rev. Letters 34, 1548 (1975).
2. J. GOREE et al., Phys. Fluids 28, 2845 (1985).
3. T.H. STIX, Theory of Plasma Waves, McGraw Hill, 1962.

EVOLUTION OF ELECTROSTATIC WAVES AND BEAM DISTRIBUTION FUNCTION IN A BEAM PLASMA SYSTEM

J.A. Michel, J.-P. Hogge, P.-J. Paris, A. Frey and M.Q. Tran

Centre de Recherches en Physique des Plasmas
Association Euratom - Confédération Suisse
Ecole Polytechnique Fédérale de Lausanne
21, Av. des Bains, CH-1007 Lausanne/Switzerland

ABSTRACT

The thermalization of an electron beam ($E_b \leq 2$ keV, $n_b/n_o \leq 1.5$ %) in a plasma is studied experimentally. It is shown that high energy beam ($E_b \approx 2$ keV) can propagate in a plasma over distance of about 1m (or 10^4 λ_{De}) before being thermalized. Under these circumstances, a zone where no Langmuir waves were excited was observed in the vicinity of the injection region. This quiescent zone is then followed by a region where Langmuir turbulence occured and at the end of which the beam thermalized.

1. INTRODUCTION

Experimental results in both magnetized[1,2] and unmagnetized[3,4] beam - plasma system have shown intense Langmuir waves generation and their collapse due to modulational instability. The relation between the development of the modulational instability and density cavities has been carefully studied. Less attention has been paid to the propagation of the beam itself in the case of strong turbulence. Theory[5] predicts the propagation of the beam over large distances and an excitation of Langmuir turbulence along the beam path. We present here an experimental investigation of the distribution function of an energetic beam injected into a steady state plasma. Measurements of electrostatic waves are also reported.

2. EXPERIMENTAL APPARATUS

A large volume (diameter: 2 m, length: 3 m) argon plasma was created by the discharge of four independent groups of each 56 tungsten filaments. The electron gun (diameter: 0.3 m) consists of Nickel strips coated with barium oxide which are directly heated. Two different sets of parameters were used:

A) n_o: $0.5 \cdot 10^{10} cm^{-3}$, T_e: 0.7 eV, n_b/n_o: 1.5 %, E_b: 2.0 KeV, V_b/V_{te} = 53.5, K_b: 2.1 cm^{-1}, beam pulse length: 5 μs.

B) n_o: $1.1 \cdot 10^{10} cm^{-3}$, T_e: 1.4 eV, n_b/n_o: 1.0 %, E_b: 1.7 KeV, V_b/V_{te} = 35, K_b: 3.5 cm^{-1}, beam pulse length: 5 μs.

V_b, V_{te}, K_b are respectively the beam velocity, the electron thermal velocity $(2\ T_e/m_e)^{1/2}$, and the K vector of the resonant wave (ω_{pe}/V_b). The values of the beam energy normalised to the plasma temperature and the ratio of the beam density over the plasma density correspond to strong turbulence regime[5] for the two sets of parameters. In order to minimize the angular spread of the beam a longitudinal magnetic field of 1.3 to 3.1 Gauss was applied. This low magnetic field has negligible effects on the experimental results. The Langmuir waves were measured by a 2 cm length cylindrical probe parallel to beam propagation. The distribution function of the beam was

measured using an analyzer constructed on the principle of the deflection of the electrons by electric field. Instead of slowing down the electrons by a high electric field as in standard multi-grid analyzer, we used a lower electric field to deflect the electrons, thus having the benefits of lower voltages and a larger gap between the polarized plates. The analyzer consists of a slot selecting a sheet of the beam electrons. Having passed this aperture, the electrons are deflected by a DC perpendicular electric field produced by two polarized plates. Finally a thin plate collects the electrons. The analyzer geometry was selected so that 6 keV beams were analysed by applying a voltage between the deflecting plate of 2.6 KV. No arcing problem was encountered up to this energy, since the maximum DC electric field required was only 100 KV/m.

3. EXPERIMENTAL RESULTS

As soon as the beam was injected, the high frequency electrostatic waves appeared in the vicinity of the cathode (Fig. 2, t=1 μs). At later times a difference in the waves propagation characteristics occurs depending on the energy of the beam. For a high energetic beam (V_b/V_{te}=53.5) we measured a displacement of the electric noise and an absence of Langmuir waves near the cathode (Fig. 2A, t=3 μs). This displacement had no correlation with the small unavoidable stationary gradient of the plasma in front of the cathode. Before the end of the injection the extend of this quiet region decreased. The beam energy and the beam spread changed only slightly up to the end of the region where Langmuir waves appeared (Fig. 1-3). Further away the beam was thermalized quickly. When the beam was switched off, all electrostatic waves damped out. This indicates that the beam supports the Langmuir waves which are along its path but it loses its energy mainly at the end of the interaction region. For lower beam energy (V_b/V_{te}=35) the interaction region remained stationary (Fig. 2B) and was limited to a small region near the cathode. As for the first case, the beam penetrates through the plasma without being thermalized until the end of the region where Langmuir waves appeared.

4. DISCUSSION AND CONCLUSIONS

In some experiments[3,4], the first electrostatic spike presents a good repetitivity from shot to shot. Our results however never showed such repetitive structure. The propagation of the lower energetic beam produced waves with a spatial structure which is similar to the one calculated by Galeev et al.[5] considering a plasma noise in resonance with the beam. But for the case of the more energetic beam this interaction region moves and near the cathode a quiescent zone takes place. A possible explanation of this absence of Langmuir waves near the cathode is the existence of density inhomogeneities resulting of the modulational instability of the Langmuir waves. A density depression[3] or low frequency plasma density fluctuations can decouple the beam from the plasma.

In summary, we measured the propagation of the interaction region between an energetic beam and a plasma. The main part of the beam energy is lost at the end of the zone in which Langmuir waves are observed. A quiescent region without high frequency electrostatic waves appeared near the cathode for high energy beams. The characteristics of the plasma in this region are under investigation.

ACKNOWLEDGMENTS - This work is partially supported by the Swiss National Science Foundation under grants 2.868-0.85 and 2.869-0.85. We acknowledge fruitful discussions with Professor M.V. Goldman, Dr. L. Muschietti and Professor R. Stern.

REFERENCES

1 S.V. Antipov et al., Physica 3D, 1981, 1 & 2, 311-328.

2 R.w. Boswell et al., Physics Letters, 1984, 101A, 9, 501-504.

3 P.Y. Cheung & A.Y. Wong, Physical Review Letters, 1985, 55, 1880-1883.

4 N.V. Astrakhantsev et al., Physics Letters, 1985, 110A, 3, 129-132.

5 A.A. Galeev et al., Sov. Phys. JETP, 1977, 45(2), 266-271.

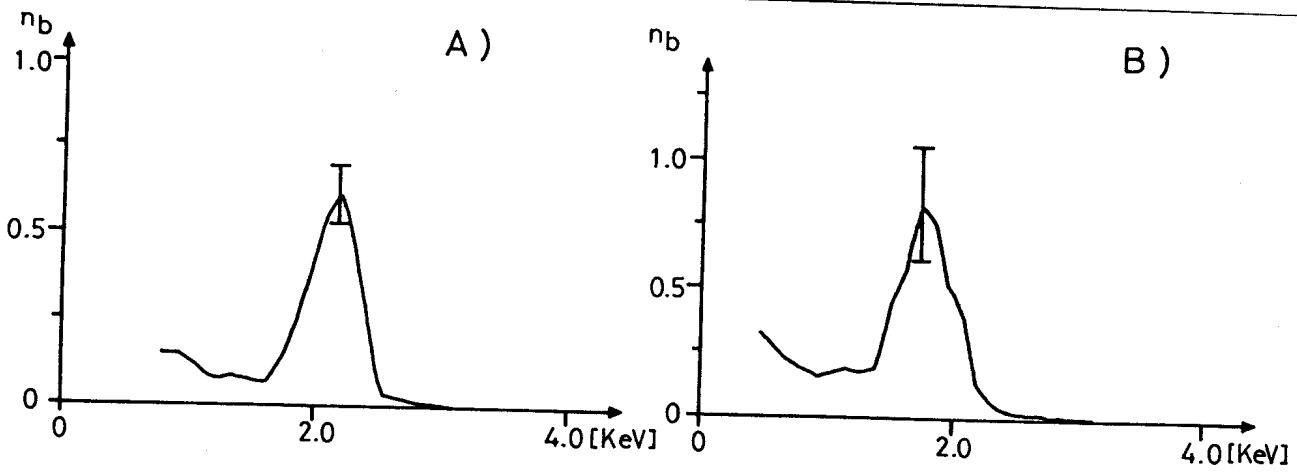

Fig. 1: Distribution function of the beam after 3 μS of injection.
A) n_b/n_o = 1.5 %, V_b/V_{te} = 53.5, z: 49 cm
B) n_b/n_o = 1.0 %, V_b/V_{te} = 35, z: 29 cm

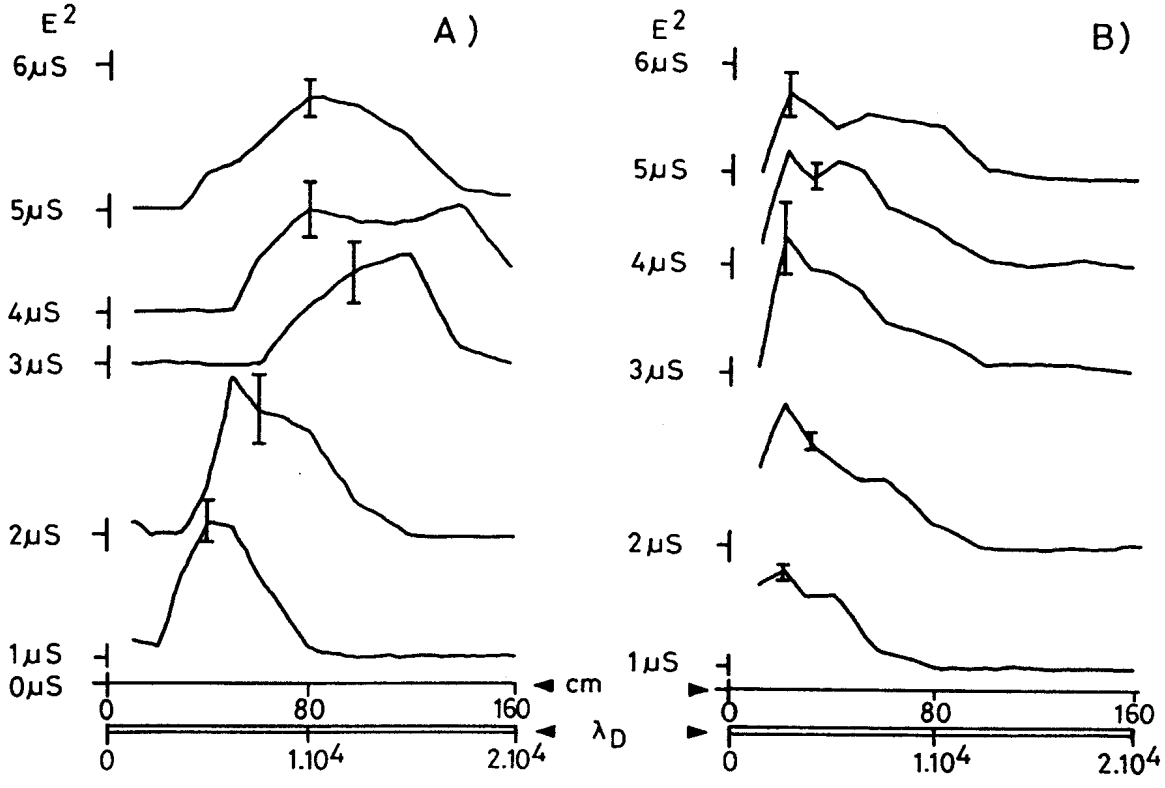

Fig. 2: Electrostatic waves intensity for different times after beam injection in function of the distance.
A) n_b/n_o = 1.5 %, V_b/V_{te} = 53.5
B) n_b/n_o = 1.0 %, B_b/V_{te} = 35

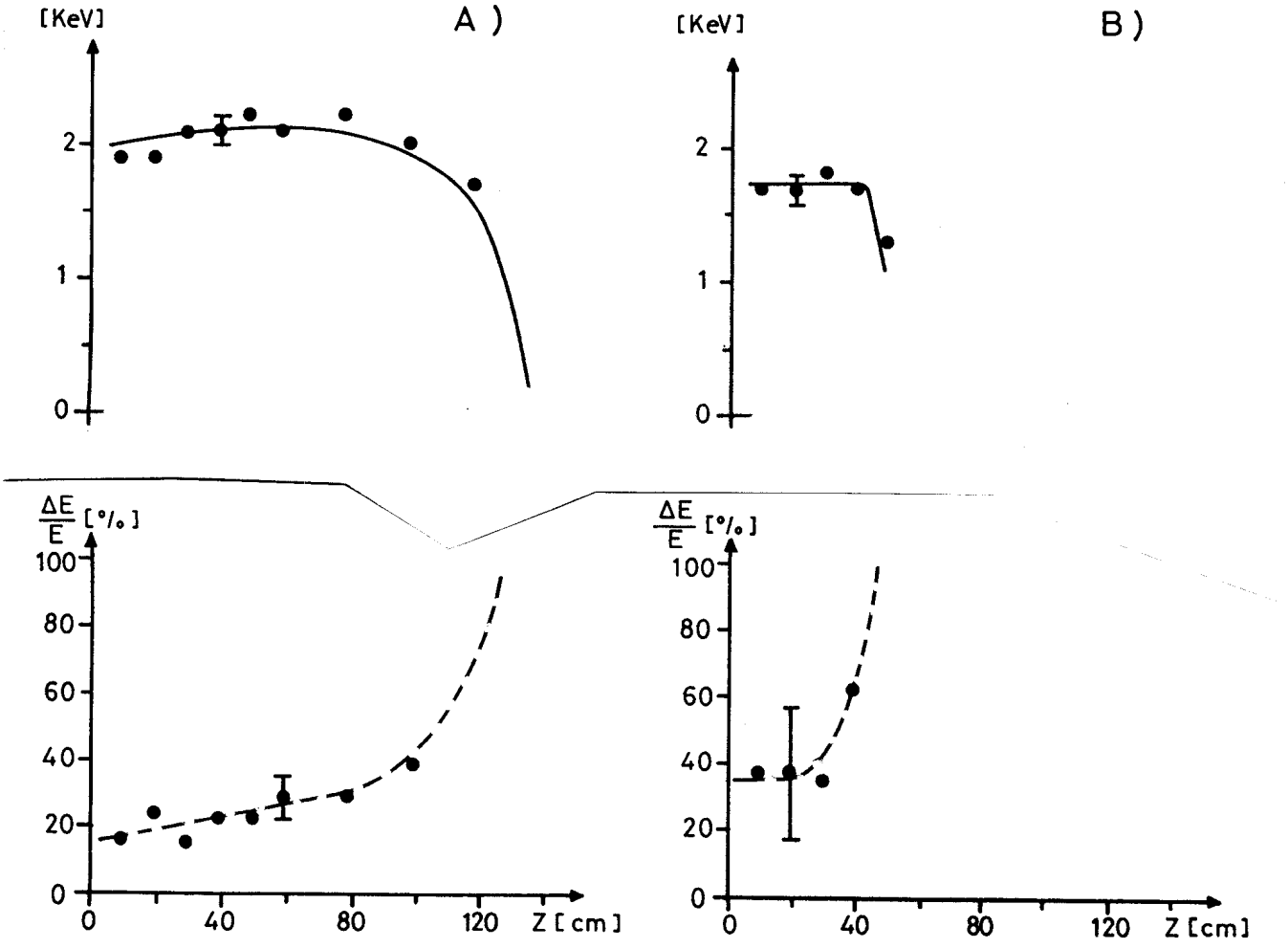

Fig. 3: Spatial dependence of the beam 3 μS after the beginning of the injection. Continuous line: beam energy, dashed line: beam width (at half height).

A) n_b/n_o = 1.5 %, V_b/V_{te} = 53.5

B) n_b/n_o = 1.0 %, B_b/V_{te} = 35